Clinical & Experimental Immunology
The Journal of Translational Immunology

Clinical and Experimental Immunology ORIGINAL ARTICLE doi:10.1111/cei.12862

Increased chemotaxis and activity of circulatory myeloid progenitor cells may contribute to enhanced osteoclastogenesis and bone loss in the C57BL/6 mouse model of collagen-induced arthritis

M. Ikić Matijašević,*†[1] D. Flegar,*†[1] N. Kovačić,†‡ V. Katavić,†‡ T. Kelava,*† A. Šućur,*† S. Ivčević,*† H. Cvija,*† E. Lazić Mosler,†‡ I. Kalajzić,§ A. Marušić¶ and D. Grčević*†

*Department of Physiology and Immunology, †Laboratory for Molecular Immunology, Croatian Institute for Brain Research, ‡Department of Anatomy, University of Zagreb School of Medicine, Zagreb, Croatia, §Department of Reconstructive Sciences, University of Connecticut Health Center, Farmington, CT, USA, and ¶Department of Research in Biomedicine and Health, University of Split School of Medicine, Split, Croatia

Accepted for publication 3 September 2016
Correspondence: D. Grčević, Department of Physiology and Immunology, University of Zagreb School of Medicine, Šalata 3b, 10000 Zagreb, Croatia.
E-mail: dgrcevic@mef.hr

[1]These authors contributed equally to this work.

Summary

Our study aimed to determine the functional activity of different osteoclast progenitor (OCP) subpopulations and signals important for their migration to bone lesions, causing local and systemic bone resorption during the course of collagen-induced arthritis in C57BL/6 mice. Arthritis was induced with chicken type II collagen (CII), and assessed by clinical scoring and detection of anti-CII antibodies. We observed decreased trabecular bone volume of axial and appendicular skeleton by histomorphometry and micro-computed tomography as well as decreased bone formation and increased bone resorption rate in arthritic mice *in vivo*. In the affected joints, bone loss was accompanied with severe osteitis and bone marrow hypercellularity, coinciding with the areas of active osteoclasts and bone erosions. Flow cytometry analysis showed increased frequency of putative OCP cells ($CD3^-B220^-NK1.1^-CD11b^{-/lo}CD117^+CD115^+$ for bone marrow and $CD3^-B220^-NK1.1^-CD11b^+CD115^+Gr\text{-}1^+$ for peripheral haematopoietic tissues), which exhibited enhanced differentiation potential *in vitro*. Moreover, the total $CD11b^+$ population was expanded in arthritic mice as well as $CD11b^+F4/80^+$ macrophage, $CD11b^+NK1.1^+$ natural killer cell and $CD11b^+CD11c^+$ myeloid dendritic cell populations in both bone marrow and peripheral blood. In addition, arthritic mice had increased expression of tumour necrosis factor-α, interleukin-6, CC chemokine ligand-2 (*Ccl2*) and *Ccl5*, with increased migration and differentiation of circulatory OCPs in response to CCL2 and, particularly, CCL5 signals. Our study characterized the frequency and functional properties of OCPs under inflammatory conditions associated with arthritis, which may help to clarify crucial molecular signals provided by immune cells to mediate systemically enhanced osteoresorption.

Keywords: bone loss, chemokines, collagen-induced arthritis, inflammation, osteoclast progenitors

Introduction

Collagen-induced arthritis (CIA) is a valuable animal model of autoimmune arthritis with the symmetrical inflammation of forepaws and hind paws that includes stiffness, redness, swelling and pain [1–4], which clinically, immunologically and pathologically resemble rheumatoid arthritis (RA) in humans. RA is hallmarked by synovial inflammation and hyperplasia, followed by cartilage damage, joint destruction and ankylosis [5]. Alongside synovitis, inflammatory infiltrate is found similarly in subchondral and periarticular bone marrow, detected by magnetic resonance imaging as bone marrow oedema (inflammation-induced fluid retention in the bone marrow compartment) and histologically as osteitis (increased vascularization and substitution of bone marrow fat by inflammatory cells) [6]. Accumulation of T and B lymphocytes, plasma cells and macrophages is associated with disease activity and development of bone erosions [7–9].

Bone loss in RA occurs locally at affected joints, and systemically in the form of osteopenia and osteoporosis. Local

changes are presented as marginal bone erosions, subchondral bone resorption and periarticular bone loss [7,8]. Osteodestruction is mediated by increased activity of osteoclasts, specialized bone-resorbing multi-nucleated cells. They originate from haematopoietic progenitors of monocyte/macrophage lineage, expressing receptors for the two crucial osteoclastogenic factors: macrophage colony-stimulating factor (M-CSF) receptor (CD115/cFms) and receptor activator of nuclear factor-κB (CD265/RANK; also known as tumour necrosis factor receptor superfamily member 11A, TNFRSF11A) [10,11]. Myeloid origin was confirmed by studies demonstrating the existence of a common monocyte progenitor able to differentiate clonally into mature functional osteoclasts, macrophages and dendritic cells with high efficiencies *in vitro* [11–14]. Osteoclastogenesis is induced by the interaction of RANK with receptor activator of nuclear factor-κB ligand (CD254/RANKL, tumour necrosis factor ligand superfamily member 11, TNFSF11), expressed on stromal cells, osteoblasts, osteocytes and hypertrophying chondrocytes, as well as on activated T lymphocytes. Osteoprotegerin (OPG, tumour necrosis factor receptor superfamily member 11B, TNFRSF11B) counteracts osteoclastogenesis acting as a soluble decoy receptor for RANKL, which prevents RANKL binding to RANK [15,16]. Osteoclast progenitors are found physiologically in the bone marrow as well as in the circulation [17]. The highly osteoclastogenic progenitor population accounts for approximately 0·1–0·3% of total nucleated bone marrow cells and resides within the $CD11b^{-/lo}CD115^{+}CD117^{+}$ immature myeloid subset. The phenotype of peripheral osteoclast progenitors corresponds to circulating monocytes, described as $CD11b^{+}Ly\text{-}6C^{hi}CD115^{+}$ cells [11–14]. Although murine osteoclast progenitors have been characterized extensively, pathways of osteoclast differentiation and activation under the inflammatory conditions associated with arthritis are less well understood.

Immune cells activated by inflammation produce a number of mediators, acting directly or indirectly to induce excessive osteoresorption [18,19]. In particular, inflammatory cytokines [interleukin (IL)-1, IL-6, IL-17, IL-18, tumour necrosis factor (TNF)-α, etc.] and chemokines (CCL2, CCL3, CCL4, CCL5, CXCL12, etc.) are produced increasingly in arthritis and, by autocrine, paracrine and endocrine mechanisms, affect the number, differentiation, migration and function of osteoclast progenitor cells [20,21]. However, molecular signals underlying systemic activation and recruitment of osteoclast progenitors to articular and extra-articular bone surfaces are not defined precisely.

In the present study we aimed to determine the frequency and differentiation potential of osteoclast progenitor subpopulations, paralleled by analysis of the dynamic changes in the local and systemic bone remodelling over the course of CIA in C57BL/6 (B6) mice. In addition, we assessed changes in myeloid cell populations and production of inflammatory mediators to identify chemotactic signals important for osteoclast progenitor migration to bone lesions and their enhanced functional activity.

Materials and methods

Induction and assessment of CIA

B6 male mice (8–10 weeks old) were used in all experiments. All experimental procedures were approved by the Ethics Committee of the University of Zagreb School of Medicine (no. 380-59-10106-14-55/151) and conducted in accordance with accepted standards of ethical care and use of laboratory animals.

For CIA induction in B6 mice, we followed a modified protocol described by Brand *et al.* [2] and Inglis *et al.* [3]. Mice, anaesthetized using tribromoethanol (Avertin), were immunized by injecting 50 μl of 2 mg/ml chicken collagen type II (CII; Sigma-Aldrich, Saint Louis, MO, USA) emulsified with complete Freund's adjuvant (FA; BD Biosciences, San Jose, CA, USA) intradermally, at the base of the tail. The emulsion contained 2 mg/ml of heat-killed *Mycobacterium tuberculosis* strain H37RA (BD Biosciences). The booster dose containing the same amount of CII emulsified with incomplete FA was applied 3 weeks later, near the earlier injection site. Control mice received phosphate-buffered saline (PBS) by the same procedure. Mice were sacrificed on day 40 (early arthritis) and day 70 (late arthritis) after primary immunization, with eight to 10 mice per group (Fig. 1a).

Visual scoring for clinical signs of arthritis was performed at 5-day intervals, starting at the time of secondary immunization by grading arthritis development in each paw: 0 = no changes, 1 = swelling and/or redness limited to one finger/toe, 2 = swelling and/or redness of more than one finger/toe, or slight paw swelling, 3 = moderate paw swelling and redness and 4 = severe paw swelling and redness with ankylosis, with the maximum clinical score of 16 per mouse [3].

Detection of anti-CII antibodies

Anti-CII antibody isotypes immunoglobulin (Ig)G1 and IgG2a were assessed in the mouse sera by enzyme-linked immunosorbent assay (ELISA) [3]. Assay was performed at room temperature; 96-well ELISA plates were coated overnight with 100 μl/well chicken CII at concentration 5 μg/ml, washed four times with PBS/0·05% Tween20, blocked for 1 h with PBS/2% bovine serum albumin (BSA), washed again and then incubated for 2 h with sera diluted 1 : 2000 in PBS. Serial dilutions of pooled sera from 10 mice with late arthritis were used to design the relative standard curve. After washing, 100 μl/well of rat anti-mouse IgG1 and IgG2a horseradish peroxidase (HRP)-conjugated antibodies (BD Biosciences) diluted 1 : 1000 in PBS/2% BSA were added and incubated for 1 h, followed by washing and adding 3,3′,5,5′-tetramethylbenzidine (Sigma-Aldrich) substrate for 15–30 min. To stop the reaction, 10 mM sulphuric acid was used. Optical density was measured

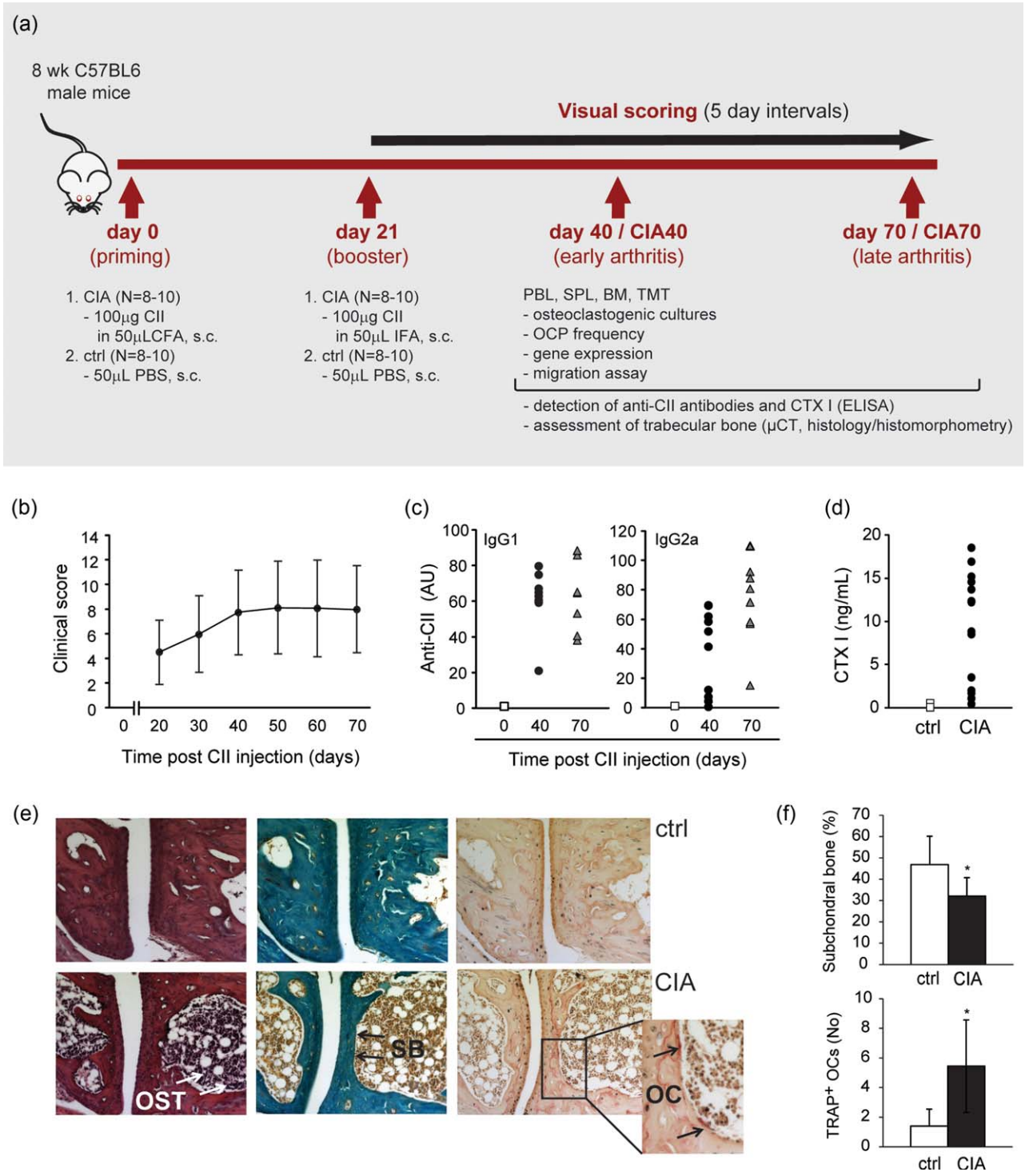

at 450 nm. Antibody concentrations were expressed with relative quantities in reference to the standard curve.

Assessment of mouse cross-linked C-telopeptide of type I collagen

Concentrations of mouse cross-linked C-telopeptide of type I collagen (CTX I) were determined in the mouse sera using a commercially available ELISA kit (Cusabio Biotech Co., Wuhan, China), according to the manufacturer's directions. Briefly, a 96-well plate was precoated with goat-anti-rabbit antibody. Samples (40 μl/well) were added with anti-CTX I antibody and HRP-conjugated CTX I, and then incubated for 1 h at 37°C. After washing, the substrate was added to the wells for 15 min at 37°C and the colour developed opposite to the amount of CTX I. After stopping the

Fig. 1. Development and assessment of collagen-induced arthritis (CIA) in C57BL/6 mice. (a) Model of CIA; arthritis was induced by chicken collagen type II (CII) emulsified with complete Freund's adjuvant (CFA), with a booster dose of CII emulsified with incomplete FA (IFA). Mice were assessed at two time-points defined as early arthritis (day 40/CIA40) and late arthritis (day 70/CIA70) for characterization of osteoclast progenitor subpopulations and analysis of bone metabolism. PBL = peripheral blood; SPL = spleen; BM = bone marrow; TMT = tarsometatarsal region of hind paws; OCP = osteoclast progenitor; CTX I = cross-linked C-telopeptide of type I collagen; μCT = micro-computed tomography (micro-CT). (b) Clinical scoring of CIA by a scale of 0–16 points (0–4 points for each paw) up to 70 days following immunization. The results shown are pooled data from six independent experiments, presented as mean ± standard deviation ($n = 8$–10 mice per group). (c) Serum levels of anti-CII immunoglobulin (Ig)G1 and IgG2a antibodies in CIA analysed by enzyme-linked immunosorbent assay (ELISA). Experiments were repeated three times, and representative results from one set of experiments are shown. Each symbol corresponds to the serum sample from individual mouse. AU = arbitrary unit. (d) Serum level of CTX I in CIA analysed by ELISA. The results shown are pooled data from three independent experiments (CIA, day 40). Each symbol corresponds to the serum sample from individual mouse. (e) Histological assessment of the first tarsometatarsal joint in mice developing arthritis (CIA, day 40) reveals osteitis and loss of subchondral bone, with prominent osteoclasts adjacent to the subchondral regions [haematoxylin and eosin (left), Goldner–Masson trichrome (middle) and tartrate-resistant acid phosphatase (TRAP) stain (right)]. Magnification ×200. OST = osteitis; SB = subchondral bone; OC = osteoclasts. (f) Histomorphometric analysis of subchondral bone volume and number of active osteoclasts in control (ctrl) and arthritic mice (CIA, day 40). The experiments were repeated three times and data from a representative experiment are shown as mean ± standard deviation ($n = 8$ mice per group). *Significant difference from control at $P < 0{\cdot}05$, Student's *t*-test. [Colour figure can be viewed at wileyonlinelibrary.com]

reaction, the optical density was measured at 450 nm. CTX I concentrations were expressed with reference to the standard curve designed using the standard vials (range = 0·075–15 ng/ml), with assay sensitivity of 0·04 ng/ml.

Osteoclastogenic cultures

Bone marrow cells and cells released from femoral and tibial bone shafts were cultured overnight with 5 ng/ml M-CSF (R&D Systems, NE Minneapolis, MN, USA) in α-minimum essential medium (MEM)/10% FCS to stimulate the monocyte/macrophage lineage, followed by harvesting of non-adherent cells as enriched haematopoietic monocyte/macrophage progenitors. Non-adherent cells were replated into 48-well plates at a density of $0{\cdot}25 \times 10^6$/well in 0·5 ml/well of α-MEM/10% FCS supplemented with 20 ng/ml M-CSF and 40 ng/ml RANKL (R&D Systems). Spleen and peripheral blood mononuclear cells [PBMC; obtained by Histopaque (Sigma-Aldrich) separation] were cultured in 48-well plates at a density of $0{\cdot}5 \times 10^6$/well in 0·5 ml/well of α-MEM/10% FCS supplemented with 20 ng/ml M-CSF and 40 ng/mL RANKL. At days 5–7 of culture, tartrate-resistant acid phosphatase (TRAP)-positive multinucleated osteoclasts (≥ three nuclei/cell) were identified using a commercially available kit (Sigma-Aldrich) and counted by light microscopy [22,23]. In selected experiments, osteoclast cultures were treated with 10 ng/ml CCL5 (PeproTech, Rocky Hill, NJ, USA).

Flow cytometry

Analysis and sorting of osteoclast progenitor cells from spleen and bone marrow were performed in a BD FACSAria I (BD Biosciences) instrument. Bone marrow cells were harvested by flushing femora and tibiae with staining medium (PBS/2% FCS) using a 23-gauge needle. Spleens were mashed gently in staining medium between a pair of frosted microscope slides. Erythrocytes were lysed with red blood cell lysing buffer (Sigma-Aldrich) and single-cell suspensions were obtained by filtering through a 100 μm Nytex mesh. Cells were counted in a haemocytometer by trypan blue exclusion and labelled using a mix of commercially available monoclonal antibodies against lymphoid lineage markers [anti-CD3 fluorescein isothiocyanate (FITC) (clone 145-2C11) for T lymphocytes, anti-B220 FITC (clone RA3-6B2) for B lymphocytes and NK1.1 FITC (clone PK136) for natural killer cells], myeloid lineage marker [anti-CD11b APC-eFluor 780 (clone M1/70)] and osteoclast progenitor markers [anti-CD115/cFms biotinylated (clone AFS98), anti-CD117/c-kit allophycocyanin (APC) (clone 2B8), anti-Gr-1 APC (clone RB6-8C5)], all from eBiosciences (San Diego, CA, USA). Suspensions were incubated on ice for 45 min, followed by washing in staining medium. As a second step (for biotinylated anti-CD115), cells were stained with streptavidin coupled to phycoerythrin-cyanin 7 (PE-Cy7) on ice for 45 min. Finally, cells were resuspended in staining medium containing 1 μg/ml propidium iodide (PI) for dead cell exclusion. Sorting gates were defined using unlabelled cells and fluorescence minus one controls. For fluorescence-activated cell sorting (FACS), labelled cells were acquired at a speed of approximately 5000 cells/s using the gating strategy described by Jacquin *et al.* [13] and Jacome-Galarza *et al.* [14]. Briefly, singlets were delineated from total cell population depicted on forward- *versus* side-scatter plot and then dead cells were excluded from the analysis based on PI incorporation, followed by plotting lymphoid markers *versus* CD11b, and subsequent dissection of CD115 *versus* CD117 expression for bone marrow or CD115 *versus* Gr-1 expression for spleen cells. Defined populations of osteoclast progenitor cells were sorted in 2 ml collection tubes containing α-MEM/20% FCS and used for osteoclastogenic cultures. Cultures were plated in a density of 5×10^3 cells/well for bone marrow and 10^4 cells/well for spleen in 96-well plates, and supplemented with 30 ng/ml M-CSF and

60 ng/ml RANKL. Sorting parameters and experimental set-up were optimized for high purity sorting. Sorting purity was determined by a reanalysis of fractioned populations and was greater than 99% for all experiments. At days 5–7 of culture, $TRAP^+$ multi-nucleated osteoclasts ($\geq$ three nuclei/cell) were counted by light microscopy [22,23].

For the phenotype characterization of spleen, PBMC and bone marrow myeloid cells, we used directly conjugated monoclonal antibodies for myeloid lineage markers (CD11b, CD11c, F4/80) (all from eBiosciences). In some experiments, a CD45 marker was used to designate the total haematopoietic population. In addition, the frequency of osteoclast progenitor subpopulations (defined as $CD3^-B220^-NK1.1^-CD11b^{-/lo}CD115^+CD117^+$ for bone marrow, $CD3^-B220^-NK1.1^-CD11b^+CD115^+Gr\text{-}1^+$ for spleen, $CD45^+CD3^-B220^-NK1.1^-CD11b^+CD115^+CD265/RANK^+$ for osteoclastogenic cultures and $CD3^-B220^-NK1.1^-CD11b^+CD115^+CD195/CCR5^+$ for migration assay; all from eBiosciences) was assessed using Attune (Life Technologies, ABI, Carlsbad, CA, USA) instrument and analysed by FlowJo software (TreeStar, Ashland, OR, USA).

Migration assay

Migration assays of PBMC were performed in 24-well Transwell plates (8·0 μm pore size) (Costar, Corning Inc., Corning, NY, USA). After stimulation with RANKL and M-CSF for 48 h, cells from control and CIA groups were seeded into the upper chamber of the Transwell system at a concentration of 10^4 cells/well in 100 μl medium, and the lower chamber was filled with 10 ng/ml CCL2 or CCL5 (PeproTech for both) in 500 μl medium. After 5 h of incubation at 37°C with 5% CO_2, the upper surface of the filters was washed carefully with PBS, and the remaining cells were removed with a cotton wool swab. The cells that migrated to the bottom side of the Transwell membrane inserts were fixed with 4% paraformaldehyde and stained with 4′,6-diamidine-2′-phenylindole dihydrochloride (DAPI). The migrated cells were counted (two wells per group, four central fields per Transwell) at ×100 magnification using a fluorescent microscope (Axiovert 200; Carl Zeiss, AG, Oberkochen, Germany).

Micro-computed tomography

The distal femoral metaphyses and second lumbar vertebrae were scanned using micro-computed tomography (micro-CT) (1172 SkyScan; Bruker, Kontich, Belgium) at 50 kV and 200 mA with a 0·5 aluminum filter using a detection pixel size of 4·3 μm. Images were captured every 0.7° through 180° (second lumbar (L2) vertebrae) and every 0·7° through 360° (femora) rotation. The scanned images were reconstructed using the SkyScan Recon software and analysed using SkyScan CTAnalyser. Three-dimensional analysis and reconstruction of trabecular bone was performed on the bone region 1–2·3 mm distal to the growth plate. The trabecular bone compartment was delineated manually from the cortical bone, and the following variables were determined: trabecular bone volume fraction (BV/TV, %), trabecular number (Tb.N/μm), trabecular thickness (Tb.Th; μm) and trabecular separation (Tb.Sp; μm).

Histology and histomorphometry

Femora and hind paws were fixed in 4% paraformaldehyde, demineralized in 14% ethylendiamine tetraacetic acid in 3% formaldehyde, dehydrated in increasing ethanol concentrations and embedded in paraffin. Six-μm sections were cut with a Leica SM 2000 R rotational microtome (Lieca SM 2000 R; Leica Biosystems, Nussloch, Germany) and stained by Goldner–Masson trichrome, haematoxylin and eosin or TRAP activity. Histomorphometric analysis was performed under Axio Imager microscope (Carl Zeiss) using the OsteoMeasure software (Osteo-Metrics, Decatur, GA, USA) [23].

For static histomorphometry, methaphyseal regions of Goldner-Masson trichrome-stained femora, 1 mm distally from the epiphyseal plate, were analysed under ×5 objective magnification. The analysed variables included trabecular volume (BV/TV), trabecular thickness (Tb.Th, μm), trabecular number (Tb.N/μm) and trabecular separation (Tb.Sp, μm). On TRAP-stained sections, osteoclasts were identified as multi-nucleated red cells placed adjacent to the bone surface. For dynamic histomorphometry, mice were injected twice with calcein, 20 mg/kg each, at days 6 and 2 prior to sacrificing. Seven-μm sections of undecalcified femora were cut using Leica cryostat and analysed under a fluorescent microscope (Axio Imager; Carl Zeiss); bone formation rate (BFR; $\mu m^3/\mu m^2$/day) was calculated automatically.

Gene expression analysis

Total RNA from cultured cells and harvested tissues [isolated haematopoietic cells and enzymatically digested tarsometatarsal region of hind paws by 0·1% collagenase (type IV, from *Clostridium histolyticum*; Sigma-Aldrich)] was extracted using TRIzol reagent (Applied Biosystems, Thermo Fisher Scientific, Waltham, MA, USA), reverse-transcribed (1 μg) to cDNA and amplified (20 ng/well in duplicate) by quantitative polymerase chain reaction (PCR) using an AB7500 (Applied Biosystems) instrument. Expression of osteoclast differentiation genes [cFms/colony stimulating factor 1 receptor (*Csf1r*), *Rank*, cathepsin K (*Ctsk*), calcitonin receptor (*Calcr*)], chemokines (*Ccl2*, *Ccl5*) and cytokines (*Il6*, *Tnf*) was determined using commercially available TaqMan Gene Expression Assays (Applied Biosystems). The expression of a specific gene was calculated according to the relative standard curve of gene expression in the calibrator sample (cDNA from

mononuclear cells or osteoclast culture), and then normalized to the expression level of the β-actin gene as an endogenous control [22,23].

Statistics

Each set of experiments was performed at least three times and data are presented as mean value ± standard deviation (s.d.). Statistical analysis of the group difference was performed using Student's *t*-test or analysis of variance (ANOVA) with Bonferroni's correction for multiple testing. Levels of anti-collagen antibodies and measurements of dynamic histomorphometry were presented as individual values with median, analysed by Mann–Whitney *U*-test. For migration assays, values were presented as median with interquartile range and compared using the Kruskal–Wallis test with Mann–Whitney for group-to-group comparisons. The methodological studies of quantitative PCR analysis suggest that the minimal difference in gene expression that could be detected reproducibly is approximately 100% [22,23]. Therefore, we assumed the change in the gene expression that is statistically significant (ANOVA, $P < 0{\cdot}05$) and more than twofold different compared with control, repeating through all experiments, as biologically significant. Correlations were assessed by Spearman's rho (ρ) coefficient with 95% confidence interval (CI). For all experiments, α-level was set at 0·05. Statistical analysis was performed using the software packages MedCalc (version 12.5; MedCalc Inc., Mariakerke, Belgium).

Results

Clinical and serological assessment of CIA

Dark brown Agouti (DBA)/1 mice, the most susceptible strain, develop CIA with a high incidence of 80–90% and very pronounced symptoms during the acute disease course. However, specific protocols for induction of CIA in the B6 strain have been developed and optimized [2–4]. Upon induction of arthritis, mice were assessed at two time-points defined as early arthritis (day 40/CIA40) and late arthritis (day 70/CIA70) for the frequency and activity of osteoclast progenitor subpopulations in parallel with the changes in bone metabolism (Fig. 1a).

By applying the modified protocols of the model of CIA in B6 mice [3,4,24], we were able to reach the arthritis incidence of approximately 50–60% in total of 14 independent experiments (approximately 200 mice). There were no signs of arthritis in any of the control (PBS-injected) animals. However, the arthritis was mild in most cases (total clinical score mean was $6{\cdot}97 \pm 3{\cdot}91$), with one or more inflamed toes per paw and without ankylosis (Fig. 1b). During the course of the disease, mice developed mainly symmetric arthritis, with more severe affection of the hind paws. Immunization to chicken collagen was confirmed by detection of circulating anti-CII antibodies (classes IgG1 and IgG2a) in serum samples taken individually at the time of termination for each time-point (Fig. 1c). Statistical analysis revealed a significant positive correlation between the serum level of anti-CII class IgG2a antibodies and clinical score of arthritis ($\rho = 0{\cdot}522$, CI = 0·169–0·756, $P = 0{\cdot}009$). Bone degradation during development of arthritis was confirmed by increased serum levels of CTX I as a metabolic marker of bone resorption (Fig. 1d).

Histological confirmation of joint destruction in CIA

Histological analysis of the hind paws in the affected animals demonstrated severe destruction of small joints of tarsometatarsal region in arthritic mice, paralleled by the increased number of active osteoclasts adjacent to the subchondral bone surfaces compared to the control group (Fig. 1e). The majority of the affected animals exhibited bone lesions accompanied by severe osteitis, with the replacement of bone marrow adipocytes with haematopoietic (inflammatory) cells, matching the bone marrow oedema described in human RA [6]. Very few mice showed profound synovial inflammation and pannus invasion of the articular cartilage, which could probably be assigned to the specific features of CIA in the B6 mouse strain [4,24,25].

Hypercellularity of bone marrow compartment was most intensive at subchondral bone regions, coinciding with the areas of active osteoclasts and bone erosions (Fig. 1e). In addition, histomorphometric analysis of the first tarsometatarsal joint revealed loss of subchondral bone and an increased number of active osteoclasts in animals affected by early CIA compared to the control group (Fig. 1f).

Systemic bone loss in CIA

In addition to local osteoclast activation and joint destruction, we aimed to confirm systemic alterations in bone metabolism paralleled by the increased osteoclast activity and enhanced bone resorption in CIA (Fig. 1d). Using micro-CT analysis, we assessed axial (at the level of L2 vertebra) and appendicular (at the level of distal femoral metaphysis) skeleton (Fig. 2a).

In early arthritis (CIA40), despite thinning of trabeculae in the L2 vertebral body (Tb.Th $42{\cdot}1 \pm 4{\cdot}4$ in control *versus* $38{\cdot}4 \pm 4{\cdot}7$ in CIA, $P = 0{\cdot}04$), the percentage of trabecular bone volume was unaffected (Fig. 2b). With the development of arthritis (CIA70), trabecular bone volume was reduced significantly (Fig. 2b) in addition to decreased trabecular thickness (Tb.Th $43{\cdot}1 \pm 6{\cdot}2$ μm in control *versus* $35{\cdot}4 \pm 2{\cdot}4$ μm in CIA, $P = 0{\cdot}001$), confirming systemic bone loss.

Appendicular skeleton was assessed by both micro-CT analysis and histology at the level of distal femoral metaphysis, showing even more prominent changes in early (CIA40) and late (CIA70) arthritis, with a significant decrease in trabecular bone volume (Fig. 2a,b), trabecular

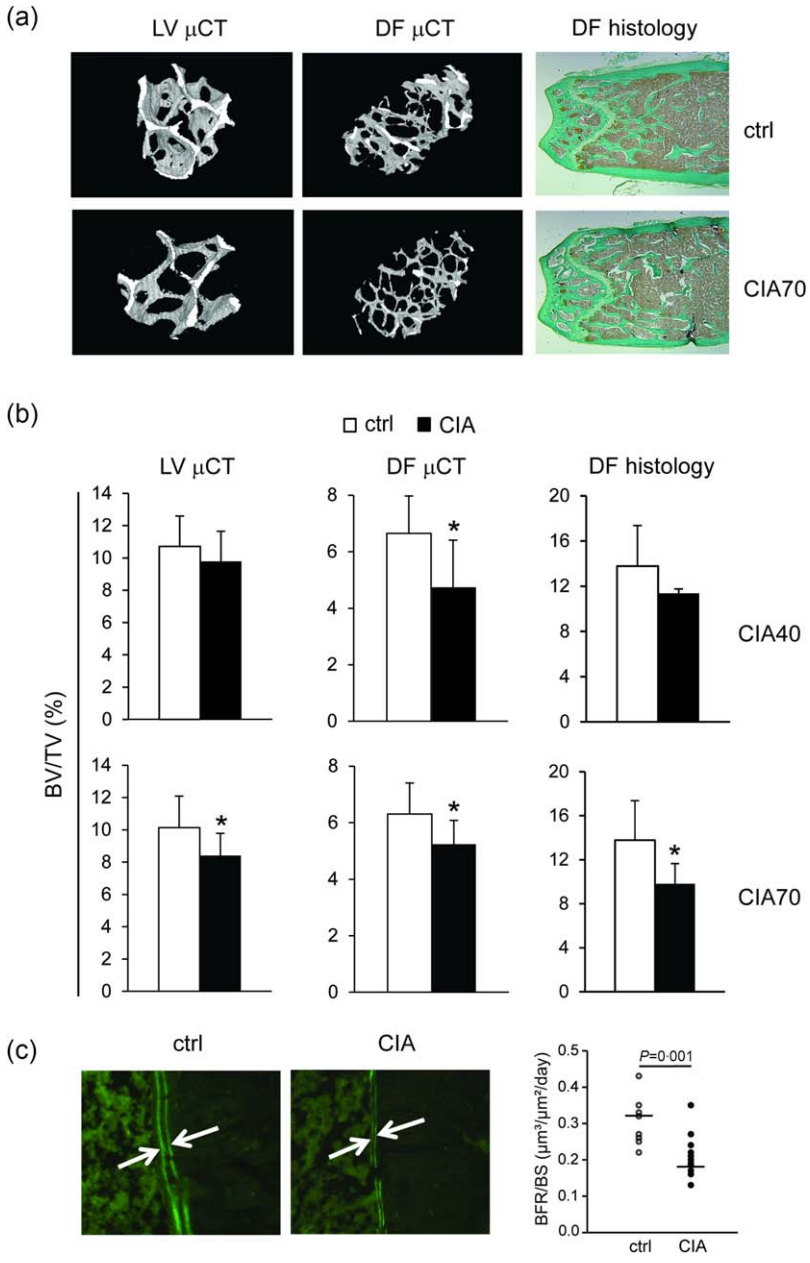

Fig. 2. Effect of collagen-induced arthritis (CIA) on bone remodelling in axial and appendicular skeleton. Second lumbar vertebra and distal femora from control (ctrl) and arthritic mice (early arthritis/CIA 40 and late arthritis/CIA70) were analysed for trabecular bone volume and bone formation rate. (a) Three-dimensional reconstruction of selected areas of the second lumbar vertebrae scanned by micro-computed tomography (μCT) (LV μCT, left) and distal femur (DF μCT, middle) and representative micrographs of distal femoral section (DF histology, right) stained with Goldner–Masson trichrome in CIA70 and control mice. (b) μCT analysis of trabecular bone volume [BV/TV (%), bone volume/total volume] in the second lumbar vertebra (LV μCT) and distal femoral metaphysis (DF μCT); histomorphometric analysis of BV/TV (%) at the level of distal femoral metaphysis (DF histology). Analysis was repeated in three independent sets of experiments for each time-point and cumulative results are shown ($n = 15$–25 mice for each group and time-point). All results are displayed as mean ± standard deviation. *Significant difference from the respective control at $P < 0{\cdot}05$, Student's *t*-test. (c) Representative microphotographs of femoral sections from control (ctrl) and arthritic mice (CIA, day 40) injected with calcein, and histomorphometric evaluation of bone formation rate relative to bone surface area (BFR/BS, $\mu m^3/\mu m^2$/day). The experiments were repeated three times and data from a representative experiment are shown ($n = 10$–13 mice per group). Symbols represent values of individual mice and horizontal lines represent median. Statistically significant difference was determined at $P < 0{\cdot}05$, Mann–Whitney *U*-test. [Colour figure can be viewed at wileyonlinelibrary.com]

thickness and trabecular number (Tb.Th 39·6 ± 4·0 μm in control *versus* 34·6 ± 5·3 μm in CIA, $P = 0{\cdot}008$ and TbN 1·64 ± 0·23/μm in control *versus* 1·36 ± 0·22/μm in CIA, $P = 0{\cdot}001$ by micro-CT). Moreover, dynamic histomophometry showed decreased bone formation rate as an indicator of suppressed osteoformation *in vivo* (Fig. 2c).

Osteoclastogenic potential of haematopoietic cells in CIA

To assess *in vitro* osteoclastogenic potential, we isolated haematopoietic cells from bone marrow, adjacent endosteal and periosteal regions, spleen and peripheral blood of mice with early arthritis, and cultured them with RANKL and M-CSF to induce differentiation of osteoclast-like multinucleated cells (Fig. 3a). The number of $TRAP^+$ osteoclasts was significantly higher in peripheral as well as bone marrow compartments in CIA compared with control animals (Fig. 3b).

As unfractionated haematopoietic tissues are heterogeneous, containing variable proportions of non-osteoclastogenic cells, we further assessed frequency and activity of defined osteoclast progenitor subpopulations according to the reports by Jacquin *et al.* [13] and Jacome-Galarza *et al.* [14]. Arthritic mice had a higher frequency of putative osteoclast progenitor cells in the bone marrow compartment, bearing the phenotype $CD3^-B220^-NK1.1^-CD11b^{-/lo}CD117^+CD115^+$ or $CD3^-B220^-NK1.1^-CD11b^{-/lo}CD117^-CD115^+$ and among

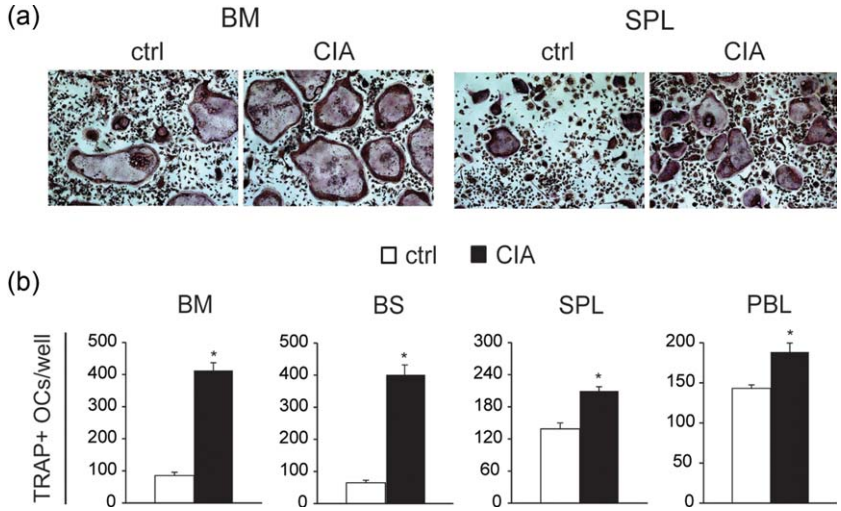

Fig. 3. Osteoclastogenic potential of mice with collagen-induced arthritis (CIA). (a) Representative microphotographs of osteoclasts differentiated *in vitro* from bone marrow (BM) and spleen (SPL) of control (ctrl) and arthritic mice (CIA, day 40), cytochemically stained for tartrate-resistant acid phosphatase (TRAP) activity. (b) Number of $TRAP^+$ osteoclasts in cultures of bone marrow (BM), cells derived from bone shaft (BS), spleen (SPL) and peripheral blood mononuclear cells (PBL), stimulated by receptor activator of nuclear factor kappa-B ligand (RANKL) and macrophage colony-stimulating factor (M-CSF) from control (ctrl) and arthritic mice (CIA, day 40). The experiments were repeated four times and data from a representative experiment are shown. Values are presented as mean ± standard deviation ($n = 4$–6 wells per group). *Significant difference from the respective control at $P < 0{\cdot}05$, Student's *t*-test. [Colour figure can be viewed at wileyonlinelibrary.com]

spleen haematopoietic cells, bearing the phenotype $CD3^-B220^-NK1.1^-CD11b^+CD115^+Gr\text{-}1^+$ (Fig. 4a). Bone marrow and spleen progenitors were FACS-sorted and confirmed to possess potent osteoclastogenic activity *in vitro*, with higher numbers of differentiated $TRAP^+$ osteoclasts in cultures from mice with CIA compared to control mice (Fig. 4b).

Studies taken as a starting-point for osteoclast progenitor dissection were performed in control (untreated) mice [13,14]. Therefore, we additionally tested osteoclastogenic efficiency of selected osteoclast progenitor subsets in the context of arthritis. Osteoclastogenic potential of lymphoid-negative cells expressing M-CSF receptor (CD115) were compared with respect to CD11b, as Jacquin *et al.* [13] reported that $CD11b^{hi}$ fraction of lymphoid-negative bone marrow cells may possess certain osteoclastogenic activity. In arthritic mice, the $CD11b^{-/lo}$ subset generated significantly more $TRAP^+$ osteoclasts compared to the $CD11b^+$ subset (300 ± 53 osteoclasts for $CD3^-B220^-NK1.1^-$ $CD11b^{-/lo}CD115^+$ cells *versus* 16 ± 6 for $CD3^-B220^-NK1.1^-CD11b^+CD115^+$ cells, $P = 0{\cdot}011$) when plated at the same density. In contrast to bone marrow, osteoclast progenitors in spleen were contained within the $CD11b^+$ subpopulation of lymphoid-negative cells, and expression of M-CSF receptor (CD115) seems to be indispensable for osteoclastogenic activity – the $CD115^+$ subset readily gave rise to $TRAP^+$ osteoclasts *in vitro* (178 ± 34 $TRAP^+$ osteoclasts for $CD3^-B220^-NK1.1^-CD11b^+CD115^+$ cells), with no osteoclastogenic activity of $CD115^-$ cells (no $TRAP^+$ osteoclasts for $CD3^-B220^-NK1.1^-CD11b^+CD115^-$ cells).

In addition to generating a higher number of $TRAP^+$ osteoclasts, differentiated osteoclast progenitors from arthritic mice exhibited enhanced expression of osteoclast-specific genes (*Rank*, *Csfr1*, *Calcr* and *Ctsk*) compared to the control, for both bone marrow and spleen (Fig. 4c). We also compared expression of early osteoclast-specific differentiation genes (*Rank* and *Csfr1*) between osteoclastogenic cultures of sorted and unfractionated bone marrow and spleen cells (Supporting information, Fig. S1). Relative *Rank* expression was higher in cultures of sorted cells, indicating that this marker is enriched specifically in osteoclast progenitor populations. Relative *Csfr1* (CD115) expression was high in unfractionated bone marrow cells and comparable between groups, due probably to the contribution of non-osteoclastogenic (myeloid) cells expressing M-CSF receptor. The more obvious difference in the expression of osteoclast-specific genes between control and arthritic samples in sorted compared to unfractionated cultures indicates enrichment of osteoclast progenitor cells.

Changes in myeloid populations and cytokine expression in CIA

As the results showed that osteoclastogenic potential was enhanced systemically in arthritis, we further assessed changes in myeloid cell populations among bone marrow and peripheral blood cells. We hypothesized that osteoclastogenic activity could be enhanced due to systemic activation of the total myeloid population (not just osteoclast progenitor cells), as a part of the autoinflammatory/autoimmune response in CIA.

Flow cytometric analysis showed expansion of the total myeloid $CD11b^+$ population in bone marrow and

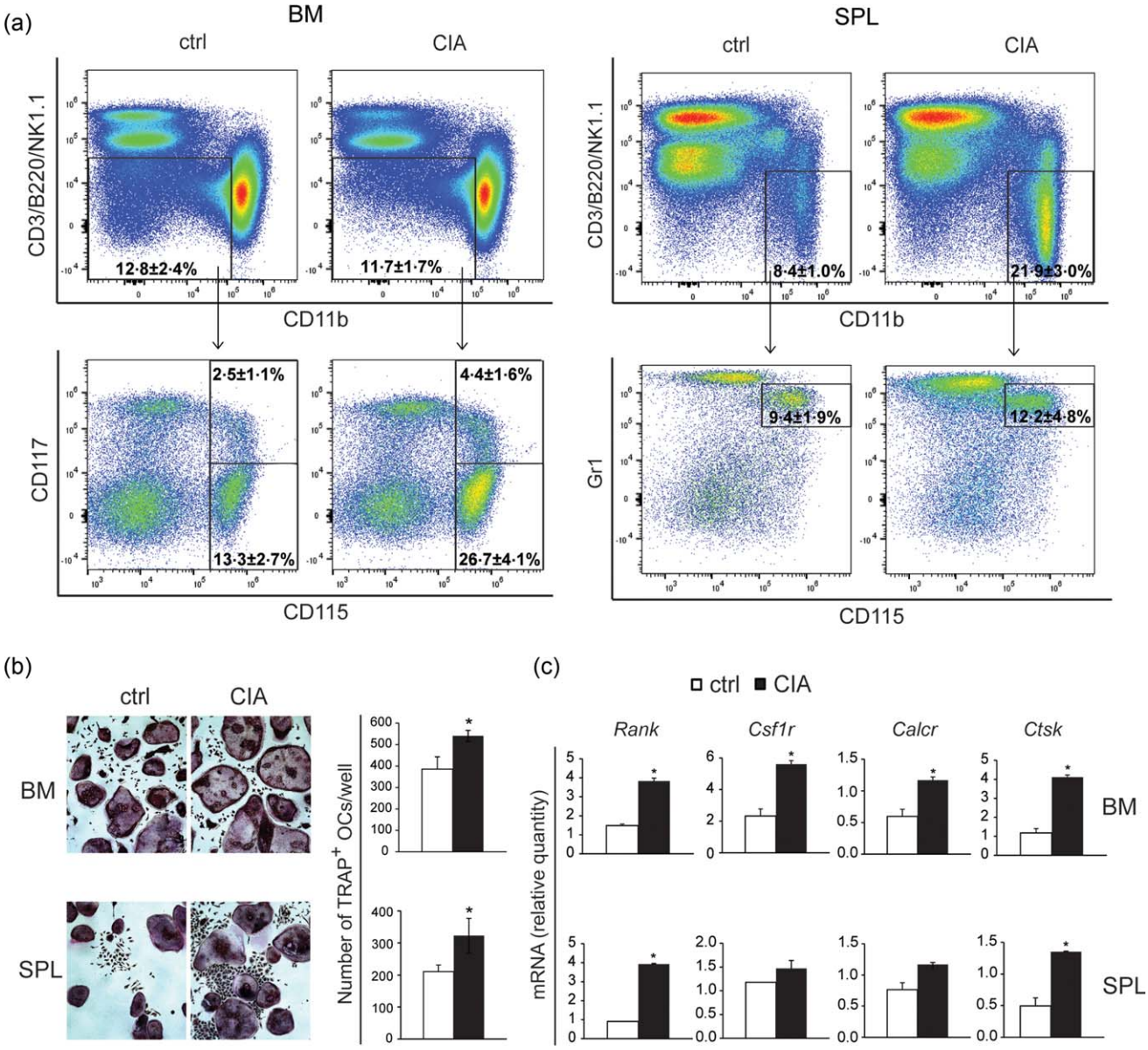

Fig. 4. Frequency and differentiation potential of sorted osteoclast progenitor cells. (a) Representative flow cytometry data of the frequency of osteoclast progenitor cells, bearing the phenotype $CD3^-B220^-NK1.1^-CD11b^{-/lo}CD115^+CD117^+$ or $CD3^-B220^-NK1.1^-CD11b^{-/lo}CD115^+CD117^-$ in bone marrow (BM); and $CD3^-B220^-NK1.1^-CD11b^+CD115^+Gr\text{-}1^+$ in spleen (SPL) of control (ctrl) and arthritic mice (CIA, day 40). Values are presented as mean ± standard deviation for three independent experiments. (b) Osteoclastogenic potential of sorted osteoclast progenitors in BM ($CD3^-B220^-NK1.1^-CD11b^{-/lo}CD115^+$) and SPL ($CD3^-B220^-NK1.1^-CD11b^+CD115^+$), stimulated by receptor activator of nuclear factor κB ligand (RANKL) and macrophage colony-stimulating factor (M-CSF), and assessed by the number of tartrate-resistant acid phosphatase $(TRAP)^+$ osteoclasts, presented as mean ± standard deviation ($n = 4$–6 wells per group). Flow cytometry analysis and sorting were performed by plotting the total cell population (excluding doublets and dead cells) for lymphoid markers *versus* CD11b, subsequently dissected for CD115 *versus* CD117 expression for BM or CD115 *versus* Gr-1 expression for SPL cells. Sorting gates were defined using unlabelled cells and fluorescence minus one controls. *Significant difference from the respective control at $P < 0{\cdot}05$, Student's *t*-test. (c) Expression of osteoclast-specific genes in osteoclastogenic cultures of sorted BM-derived and SPL-derived osteoclast progenitors, isolated from control (ctrl) and arthritic mice (CIA, day 40). Relative RNA quantities were presented as mean ± standard deviation ($n = 4$–6 wells per group). *Biologically significant difference in the expression (≥ 100%) in comparison to the respective control group. *Csf1r* = colony stimulating factor 1 receptor (CD115/cFms); *Rank* = receptor activator of nuclear factor κB; *Calcr* = calcitonin receptor; *Ctsk* = cathepsin K. [Colour figure can be viewed at wileyonlinelibrary.com]

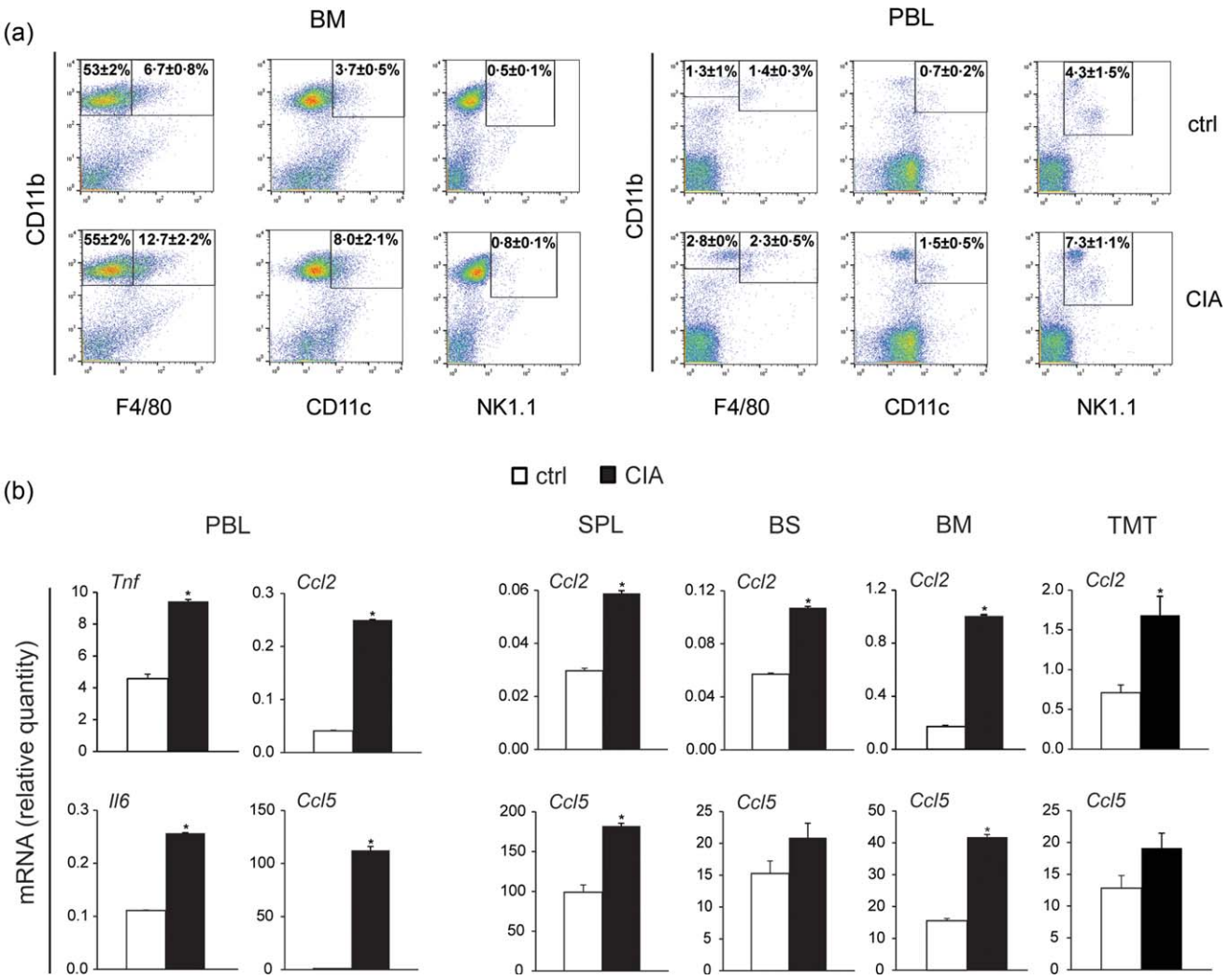

Fig. 5. Changes of myeloid cell population frequencies and inflammatory cytokine/chemokine expressions associated with arthritis. (a) Representative flow cytometry data of the frequency of myeloid subpopulations in early arthritis (CIA, day 40): myeloid lineage ($CD11b^+$), macrophages ($CD11b^+F4/80^+$), myeloid dendritic cells ($CD11b^+CD11c^+$) and natural killer cells ($CD11b^+NK1.1^+$) in bone marrow (BM) and peripheral blood mononuclear cells (PBL). Values are presented as mean ± standard deviation for three independent experiments. (b) Gene expression of tumour necrosis factor-α (*Tnf*) and interleukin-6 (*Il6*) in PBL, and chemokine ligands *Ccl2* and *Ccl5* in PBL, spleen (SPL), cells derived from bone shaft (BS), BM and tarsometatarsal region of hind paws (TMT) from control (ctrl) and arthritic mice (CIA, day 40). Relative RNA quantities were presented as mean ± standard deviation ($n = 3$ replicates for representative set of experiments). *Biologically significant difference in the expression (≥ 100%) in comparison to the respective control group. [Colour figure can be viewed at wileyonlinelibrary.com]

peripheral blood (Fig. 5a). In relation to specific myeloid subpopulations, higher percentages associated with arthritis were noticed for $CD11b^+F4/80^+$ macrophage, $CD11b^+NK1.1^+$ natural killer cell and $CD11b^+CD11c^+$ myeloid dendritic cell populations.

Finally, we assessed the expression of several cytokines and chemokines known to be associated with the systemic proinflammatory state which could, at the same time, be responsible for the enhanced activity of myeloid lineage cells that comprise osteoclast progenitors [17,18,21,26]. *Tnf*, *Il6*, *Ccl2* and *Ccl5* were expressed increasingly in PBMCs from mice developing arthritis compared to controls (Fig. 5b). Similar changes of *Ccl2* and *Ccl5* expression were observed for spleen and bone marrow cells as well as for tarsometatarsal region of hind paws (Fig. 5b).

Effects of CCL2 and CCL5 on osteoclast progenitor migration and differentiation

In the last set of experiments we evaluated the effects of CCL2 and CCL5 on circulatory osteoclast progenitor cells. These chemokines were able to cause enhanced migration of activated peripheral blood osteoclast progenitors in the migration assay

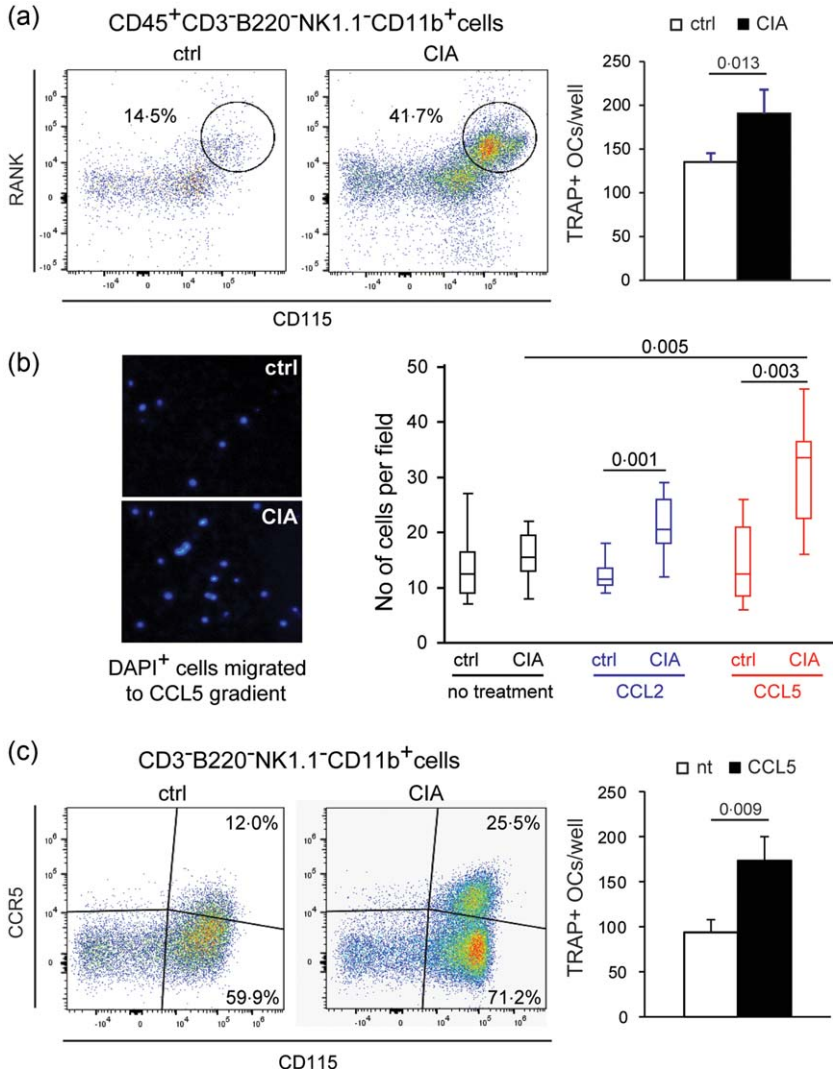

Fig. 6. *In vitro* chemotactic assay of peripheral blood mononuclear cells in collagen-induced arthritis. (a) Frequency of committed osteoclast progenitor cells $CD45^+CD3^-B220^-NK1.1^-CD11b^+CD115^+$expressing receptor activator of nuclear factor κB (RANK) (day 2 of culture) assessed by flow cytometry and the number of tartrate-resistant acid phosphatase $(TRAP)^+$ osteoclasts (day 6 of culture) differentiated in osteoclastogenic cultures ($n = 5$–6 wells per group) derived from peripheral blood mononuclear cells of control (ctrl) and arthritic mice (CIA, day 40), stimulated by receptor activator of nuclear factor κB ligand (RANKL) and macrophage colony stimulating factor (M-CSF). Statistically significant difference was determined at $P < 0{\cdot}05$, Student's *t*-test. (b) Representative images of CCL5-attracted peripheral blood mononuclear cells [nuclei stained with 4′,6-diamidino-2-phenylindole (DAPI)], prestimulated by RANKL and M-CSF, and incubated in the Transwell culture system (left). Quantitative assessment of *in vitro* cell migration ($n =$ two wells per group; four fields per well) towards CCL2 and CCL5 gradient for control (ctrl) and arthritic mice (CIA, day 40) (right). Values are presented by box and whiskers plots (horizontal lines indicate the median number of cells per field; boxes indicate interquartile range; bars indicate the minimum and maximum values). Statistically significant difference was determined at $P < 0{\cdot}05$ by Kruskal–Wallis test with Mann–Whitney for group-to-group comparisons. (c) Expression of CCR5 chemokine receptor on peripheral blood osteoclast progenitor cells ($CD3^-B220^-NK1.1^-CD11b^+CD115^+$) assessed by flow cytometry and the number of $TRAP^+$ osteoclasts (day 6 of culture) differentiated in osteoclastogenic cultures ($n =$ four wells per group) derived from peripheral blood mononuclear cells of mice with early arthritis (CIA, day 40), stimulated by RANKL and M-CSF, treated with CCL5 (10 ng/ml). Statistically significant difference was determined at $P < 0{\cdot}05$, Student's *t*-test; nt = no treatment. [Colour figure can be viewed at wileyonlinelibrary.com]

in vitro. PBMCs from mice developing early arthritis, stimulated by RANKL and M-CSF for 48 h, contained an expanded population of committed osteoclast progenitors, bearing the phenotype $CD45^+CD3^-B220^-NK1.1^-CD11b^+CD115^+RANK^+$ (Fig. 6a). In addition to the higher osteoclastogenic potential *in vitro* (Fig. 6a), these cells from arthritic mice exhibited stronger chemotaxis towards CCL2 and, particularly, CCL5 gradient compared to the respective non-arthritic controls and the arthritic group not treated with chemokines (Fig. 6b).

Population of circulatory osteoclast progenitor cells expressing CCR5 (CCL5 receptor) was enlarged in arthritic mice (Fig. 6c), explaining their higher susceptibility to

CCL5 gradient. Moreover, CCL5 exhibited direct osteoclastogenic effect by increasing the number of differentiated $TRAP^+$ cells upon addition to M-CSF/RANKL-stimulated cultures (Fig. 6c), supporting the hypothesis that once they are attracted to the inflamed joints, osteoclast progenitors could be enhanced further in their differentiation by proinflammatory chemokines.

Discussion

Although it is known that there is a systemic enhancement of osteoclast activity and generalized bone loss in addition to local joint destruction, even in patients with early RA [7,8], the precise mechanisms of osteoclast progenitor migration and activation in arthritis as well as functional relations between circulatory and local osteoclast progenitor populations have not been revealed fully. Several studies have attempted to define the phenotype of putative osteoclast progenitor cells within the myeloid lineage population of bone marrow, spleen and PBMC pools [11–14,27]. It has been demonstrated that the lymphoid-negative $CD11b^{-/lo}$ fraction recapitulates the early osteoclastogenic activity of total bone marrow [13,14], whereas reports are still inconsistent regarding the osteoclastogenic efficiency of $CD11b^+$ bone marrow cells [11,13,28]. In addition to these findings, we observed high osteoclastogenic potential of the $CD3^-B220^-NK1.1^-CD11b^{-/lo}$ fraction and inefficiency of the $CD3^-B220^-NK1.1^-CD11b^+$ bone marrow subset to form $TRAP^+$ osteoclasts *in vitro* in the context of arthritis. Jacome-Galarza *et al.* showed further that most of the osteoclastogenic activity of $CD3^-B220^-CD11b^{-/lo}$ fraction was included in the $CD115^{hi}CD117^{hi}$ population, able to generate bone-resorbing osteoclasts at a clonal level [14]. CD115/cFms, the receptor for M-CSF, is expressed on myeloid lineage cells including osteoclast progenitors, whereas the CD117/c-kit, the receptor for stem cell factor, is a consistent marker of early haematopoietic fraction [12–14]. This distinct subset of the most potent osteoclastogenic cells in bone marrow, bearing the phenotype $CD3^-B220^-NK1.1^-CD11b^{-/lo}CD115^+CD117^+$, was expanded under the inflammatory condition associated with arthritis. Monocyte progenitors with osteoclastogenic activity were also confirmed in spleen and peripheral blood [11,14,29–31]. In contrast to bone marrow, the peripheral osteoclastogenic activity is contained within the $CD11b^+$ fraction of lymphoid-negative ($CD3^-B220^-NK1.1^-$) cells [14]. Further dissection of this fraction revealed that $CD115^+Ly6C^{hi}$ cells exhibited the highest potential to form osteoclasts *in vitro*. This distinct phenotype is consistent with peripheral inflammatory-type circulating monocytes [14]. By using the similar approach to define peripheral osteoclast progenitors, we observed enlargement of the $CD3^-B220^-NK1.1^-CD11b^+CD115^+Gr\text{-}1^+$ subset in arthritic mice. These peripheral $CD11b^+CD115^+Gr\text{-}1^+$ osteoclast progenitors overlap phenotypically with the myeloid-derived suppressor cells, which have been shown to differentiate into osteoclasts contributing to bone erosions in CIA [29]. Moreover, the $CD3^-B220^-NK1.1^-CD11b^+CD115^+RANK^+$-committed osteoclast progenitor population was enlarged significantly in CIA after stimulation of PBMCs *in vitro* with RANKL and M-CSF. De Klerck *et al.*, using CIA established in the IFN-γR knock-out mice, observed a higher number of $CD11b^+RANK^+$ splenocytes, possibly serving as a source of osteoclasts responsible for bone destruction [30]. Another study using the CIA model revealed that *in vivo* depletion of $CD11b^+Gr\text{-}1^+CCR2^+$ monocytes by anti-CCR2 antibody attenuated the severity of arthritis significantly [31]. In the human TNF-α transgenic (hTNF-Tg) mouse model, a significant increase in the proportion of bone marrow and peripheral blood $CD11b^+Gr\text{-}1(Ly6G)^{-/lo}$ cells was observed [28]. Osteoclast progenitors, identified as the $CD3^-B220^-Ter119^-CD11b^{-/lo}Ly6C^{hi}$ population, were expanded in the bone marrow of the Sakaguchi mouse model of inflammatory arthritis, and had the capacity to differentiate into multi-nucleated bone-resorbing osteoclasts *in vitro* and *in vivo* [32].

In addition to osteoclast progenitor cells, myeloid lineage is induced in general as a part of autoinflammatory and autoimmune responses in CIA [26]. In our study, changes of myeloid lineage included the total $CD11b^+$ population as well as subsets of $CD11b^+F4/80^+$ macrophages and $CD11b^+CD11c^+$ myeloid dendritic cells. Monocyte/macrophage and dendritic cells contribute to arthritis pathogenesis by serving as antigen-presenting cells for xenogeneic collagen and by secreting proinflammatory cytokines, including IL-1, IL-6 and TNF-α [26,31,33]. A systemic increase in TNF-α mediated an enlargement of the peripheral $CD11b^{hi}CD115^+$ osteoclast progenitor population in the hTNF-Tg mouse model [34]. In a similar mouse model Binder *et al.* found that anti-TNF therapy reduced the number of $CD115^+$ osteoclast progenitors and intensity of subchondral lesions, without a significant impact on synovial inflammation [35]. Maintenance of the expanded osteoclast progenitor number and sustained osteoclast renewal is crucial to enable osteoclasts, whose individual lifespan is approximately 2–4 weeks, to create bone erosions during the chronic course of arthritis [36].

Osteoclastogenic assays of sorted osteoclast progenitor cells further showed greater differentiation potential and higher expression of osteoclast-specific genes in cultures obtained from arthritic mice. Under pathological osteoresorptive conditions, systemically activated osteoclast progenitors can respond to chemokine signals and home efficiently to bone surfaces causing bone resorption [8]. Expression of *Ccl2* and *Ccl5* was enhanced in our model of CIA, and both chemokines have been shown to be involved in the pathogenesis of RA [21,37,38]. CCL2 is produced within the affected joints by different cell types (including macrophages, endothelial cells, synovial fibroblasts and chondrocytes) and is elevated in synovial fluid and serum of RA patients [39]. Talbot *et al.* showed the importance of the CCR2/CCL2 interaction for neutrophil infiltration in the model of antigen-induced arthritis [40]. CCL5 could be released by inflammatory cells as well as by osteoclasts,

osteoblasts and chondrocytes [41,42], and may attract osteoclast progenitors to the sites of inflammation. In our study the migration assay identifies CCL5 and, to a lesser extent, CCL2 as potent chemotactic factors for committed osteoclast progenitors isolated from PBMC of arthritic mice. In addition, CCL5 exhibited direct osteoclastogenic effects on differentiation of peripheral blood osteoclast progenitors, which expressed CCR5 (receptor for CCL5) in significant proportion. CCR5 expression was observed on synovial tissue macrophages and synovial fluid-derived monocytes in patients with RA [43]. Moreover, CCL5 was significantly higher in synovium of RA patients compared to patients with osteoarthritis [44], and the anti-CCR5 antibody was able to block CCL5-induced chemotaxis of peripheral blood RA monocytes [45]. The susceptibility of osteoclast progenitors to chemotactic signals and increased production of respective chemokines create optimal conditions for enhanced homing of osteoclast progenitors not only to affected joints, but also at the systemic level, explaining local as well as systemic bone loss.

In addition to proinflammatory chemokines, we observed enhanced expression of *Tnf* and *Il6* in haematopoietic cells derived from bone marrow as well as from circulation. Even a small increase in systemic inflammation may trigger a self-amplifying proinflammatory state, leading to increased osteoclast activation and exaggerated bone loss [11,17,35,38,46,47]. Within the affected joints, thinning of the articular cartilage and loss of subchondral bone were most prominent in the tarsometatarsal regions, similar to previous studies on the CIA model in B10.RIII and DBA/1 mice [31]. In contrast to profound pannus invasion of the articular cartilage seen in DBA/1 strain [3–5,24], joint pathology in B6 mice is characterized by pronounced osteitis within the subchondral compartment, coinciding with the areas of $TRAP^+$ osteoclasts adjacent to the subchondral bone surfaces. As well as local changes, systemic bone loss of axial and appendicular skeleton was observed in different rodent models of arthritis [48–50]. In our model, *in vivo* bone formation was suppressed and bone resorption was enhanced resulting in decreased trabecular bone volume. Enhanced production of proinflammatory cytokines (including IL-1, IL-6 and TNF-α) is known to suppress osteoblasts function, leaving them unable to compensate for excessive osteoclast activity and bone resorption [7,19].

In conclusion, the model of CIA in B6 mouse strain seems to be particularly useful to study changes within the subchondral compartment (including osteitis and subchondral bone loss) of the affected joints in the absence of prominent synovial hyperplasia. The altered cytokine and chemokine milieu created by inflammatory and immune cells within the subchondral compartment may be crucial for the recruitment of osteoclast progenitors and activation of bone-resorbing osteoclasts. Inflammatory mediators produced by accumulated cells egress into circulation, thereby producing a systemic impact on osteoresorption, not only in arthritis but also in other inflammatory processes. In this context, characterization of osteoclast progenitors could be used to monitor disease progression and intensity of bone resorption.

Acknowledgements

We thank Professor Hector Leonardo Aguila for critical discussion of the FACS data. We also thank Ms Katerina Zrinski-Petrovic for her technical assistance. This work was supported by the Croatian Science Foundation under the project 5699.

Author contributions

I. K., A. M. and D. G. designed the study; M. I. M., D. F., S. I., N. K., V. K. and T. K. performed the experiments; M. I. M., D. F., N. K., V. K., T. K., A. Š., S. I., H. C. and E. L. M. acquired and analysed the data; A. Š., H. C., E. L. M., I. K., A. M. and D. G. interpreted the results; M. I. M., D. F. and D. G. prepared the manuscript. All authors critically revised the manuscript and approved the final version.

Disclosure

The authors declare no conflicts of interest.

References

1 Bevaart L, Vervoordeldonk MJ, Tak PP. Evaluation of therapeutic targets in animal models of arthritis: how does it relate to rheumatoid arthritis? Arthritis Rheum 2010; **62**:2192–205.
2 Brand DD, Latham KA, Rosloniec EF. Collagen-induced arthritis. Nat Protoc 2007; **2**:1269–75.
3 Inglis JJ, Simelyte E, McCann FE, Criado G, Williams RO. Protocol for the induction of arthritis in C57BL/6 mice. Nat Protoc 2008; **3**:612–8.
4 Campbell IK, Hamilton JA, Wicks IP. Collagen-induced arthritis in C57BL/6 (H-2b) mice: new insights into an important disease model of rheumatoid arthritis. Eur J Immunol 2000; **30**: 1568–75.
5 Holmdahl R, Malmstrom V, Burkhardt H. Autoimmune priming, tissue attack and chronic inflammation – the three stages of rheumatoid arthritis. Eur J Immunol 2014; **44**:1593–9.
6 Duer-Jensen A, Horslev-Petersen K, Hetland ML *et al.* Bone edema on magnetic resonance imaging is an independent predictor of rheumatoid arthritis development in patients with early undifferentiated arthritis. Arthritis Rheum 2011; **63**:2192–202.
7 Deal C. Bone loss in rheumatoid arthritis: systemic, periarticular, and focal. Curr Rheumatol Rep 2012; **14**:231–7.
8 Goldring SR, Purdue PE, Crotti TN *et al.* Bone remodelling in inflammatory arthritis. Ann Rheum Dis 2013; **72 Suppl 2**:ii52–5.
9 Bugatti S, Manzo A, Bombardieri M *et al.* Synovial tissue heterogeneity and peripheral blood biomarkers. Curr Rheumatol Rep 2011; **13**:440–8.
10 Asagiri M, Takayanagi H. The molecular understanding of osteoclast differentiation. Bone 2007; **40**:251–64.

11 Sucur A, Katavic V, Kelava T, Jajić Z, Kovačić N, Grčević D. Induction of osteoclast progenitors in inflammatory conditions: key to bone destruction in arthritis. Int Orthop 2014; **38**:1893–903.

12 Miyamoto T, Ohneda O, Arai F *et al.* Bifurcation of osteoclasts and dendritic cells from common progenitors. Blood 2001; **98**: 2544–54.

13 Jacquin C, Gran DE, Lee SK, Lorenzo JA, Aguila HL. Identification of multiple osteoclast precursor populations in murine bone marrow. J Bone Miner Res 2006; **21**:67–77.

14 Jacome-Galarza CE, Lee SK, Lorenzo JA, Aguila HL. Identification, characterization, and isolation of a common progenitor for osteoclasts, macrophages, and dendritic cells from murine bone marrow and periphery. J Bone Miner Res 2013; **28**:1203–13.

15 Walsh MC, Choi Y. Biology of the RANKL–RANK–OPG system in immunity, bone, and beyond. Front Immunol 2014; **5**:511.

16 Guerrini MM, Takayanagi H. The immune system, bone and RANKL. Arch Biochem Biophys 2014; **561**:118–23.

17 Adamopoulos IE, Mellins ED. Alternative pathways of osteoclastogenesis in inflammatory arthritis. Nat Rev Rheumatol 2015; **11**:189–94.

18 Souza PP, Lerner UH. The role of cytokines in inflammatory bone loss. Immunol Invest 2013; **42**:555–622.

19 Baum R, Gravallese EM. Impact of inflammation on the osteoblast in rheumatic diseases. Curr Osteoporos Rep 2014; **12**:9–16.

20 Braun T, Zwerina J. Positive regulators of osteoclastogenesis and bone resorption in rheumatoid arthritis. Arthritis Res Ther 2011; **13**:235.

21 Szekanecz Z, Koch AE. Successes and failures of chemokine-pathway targeting in rheumatoid arthritis. Nat Rev Rheumatol 2016; **12**:5–13.

22 Cvija H, Kovacic N, Katavic V *et al.* Chemotactic and immunoregulatory properties of bone cells are modulated by endotoxin-stimulated lymphocytes. Inflammation 2012; **35**:1618–31.

23 Kovacic N, Grcevic D, Katavic V *et al.* Fas receptor is required for estrogen deficiency-induced bone loss in mice. Lab Invest 2010; **90**:402–13.

24 Kai H, Shibuya K, Wang Y *et al.* Critical role of M. tuberculosis for dendritic cell maturation to induce collagen-induced arthritis in H-2b background of C57BL/6 mice. Immunology 2006; **118**:233–9.

25 Pan M, Kang I, Craft J, Yin Z. Resistance to development of collagen-induced arthritis in C57BL/6 mice is due to a defect in secondary, but not in primary, immune response. J Clin Immunol 2004; **24**:481–91.

26 Billiau A, Matthys P. Collagen-induced arthritis and related animal models: how much of their pathogenesis is auto-immune, how much is auto-inflammatory? Cytokine Growth Factor Rev 2011; **22**:339–44.

27 Muto A, Mizoguchi T, Udagawa N *et al.* Lineage-committed osteoclast precursors circulate in blood and settle down into bone. J Bone Miner Res 2011; **26**:2978–90.

28 Yao Z, Li P, Zhang Q *et al.* Tumor necrosis factor-alpha increases circulating osteoclast precursor numbers by promoting their proliferation and differentiation in the bone marrow through up-regulation of c-Fms expression. J Biol Chem 2006; **281**:11846–55.

29 Zhang H, Huang Y, Wang S *et al.* Myeloid-derived suppressor cells contribute to bone erosion in collagen-induced arthritis by differentiating to osteoclasts. J Autoimmun 2015; **65**:82–9.

30 De Klerck B, Carpentier I, Lories RJ *et al.* Enhanced osteoclast development in collagen-induced arthritis in interferon-gamma receptor knock-out mice as related to increased splenic CD11b+ myelopoiesis. Arthritis Res Ther 2004; **6**:R220–31.

31 Brühl H, Cihak J, Plachý J *et al.* Targeting of Gr-1+,CCR2+ monocytes in collagen-induced arthritis. Arthritis Rheum 2007; **56**:2975–85.

32 Charles JF, Hsu L-Y, Niemi EC, Weiss A, Aliprantis AO, Nakamura MC. Inflammatory arthritis increases mouse osteoclast precursors with myeloid suppressor function. The J Clin Invest 2012; **122**:4592–605.

33 Khan S, Greenberg JD, Bhardwaj N. Dendritic cells as targets for therapy in rheumatoid arthritis. Nat Rev Rheumatol 2009; **5**:566–71.

34 Li P, Schwarz EM, O'Keefe RJ *et al.* Systemic tumor necrosis factor alpha mediates an increase in peripheral CD11bhigh osteoclast precursors in tumor necrosis factor alpha-transgenic mice. Arthritis Rheum 2004; **50**:265–76.

35 Binder NB, Puchner A, Niederreiter B *et al.* Tumor necrosis factor-inhibiting therapy preferentially targets bone destruction but not synovial inflammation in a tumor necrosis factor-driven model of rheumatoid arthritis. Arthritis Rheum 2013; **65**:608–17.

36 Le Goff B, Berthelot JM, Maugars Y, Heymann D. Osteoclasts in RA: diverse origins and functions. Joint Bone Spine 2013; **80**: 586–91.

37 Kim MS, Magno CL, Day CJ, Morrison NA. Induction of chemokines and chemokine receptors CCR2b and CCR4 in authentic human osteoclasts differentiated with RANKL and osteoclast like cells differentiated by MCP-1 and RANTES. J Cell Biochem 2006; **97**:512–8.

38 Ikić M, Jajić Z, Lazić E *et al.* Association of systemic and intra-articular osteoclastogenic potential, pro-inflammatory mediators and disease activity with the form of inflammatory arthritis. Int Orthop 2014; **38**:183–92.

39 Kim MS, Day CJ, Selinger CI, Magno CL, Stephens SR, Morrison NA. MCP-1-induced human osteoclast-like cells are tartrate-resistant acid phosphatase, NFATc1, and calcitonin receptor-positive but require receptor activator of NFkappaB ligand for bone resorption. J Biol Chem 2006; **281**:1274–85.

40 Talbot J, Bianchini FJ, Nascimento DC *et al.* CCR2 expression in neutrophils plays a critical role in their migration into the joints in rheumatoid arthritis. Arthritis Rheumatol 2015; **67**: 1751–9.

41 Huh YH, Lee G, Lee KB, Koh JT, Chun JS, Ryu JH. HIF-2α-induced chemokines stimulate motility of fibroblast-like synoviocytes and chondrocytes into the cartilage-pannus interface in experimental rheumatoid arthritis mouse models. Arthritis Res Ther 2015; **17**:302.

42 Yano S, Mentaverri R, Kanuparthi D *et al.* Functional expression of beta-chemokine receptors in osteoblasts: role of regulated upon activation, normal T cell expressed and secreted (RANTES) in osteoblasts and regulation of its secretion by osteoblasts and osteoclasts. Endocrinology 2005; **146**:2324–35.

43 Katschke KJ Jr, Rottman JB, Ruth JH *et al.* Differential expression of chemokine receptors on peripheral blood, synovial fluid, and synovial tissue monocytes/macrophages in rheumatoid arthritis. Arthritis Rheum 2001; **44**:1022–32.

44 Yoshida S, Arakawa F, Higuchi F *et al.* Gene expression analysis of rheumatoid arthritis synovial lining regions by cDNA microarray combined with laser microdissection: up-regulation of

inflammation-associated STAT1, IRF1, CXCL9, CXCL10, and CCL5. Scand J Rheumatol 2012; **41**:170–9.

45 Lebre MC, Vergunst CE, Choi IY *et al.* Why CCR2 and CCR5 blockade failed and why CCR1 blockade might still be effective in the treatment of rheumatoid arthritis. PLOS ONE 2011; **6**: e21772.

46 Totoson P, Maguin-Gaté K, Nappey M, Wendling D, Demougeot C. Endothelial dysfunction in rheumatoid arthritis: mechanistic insights and correlation with circulating markers of systemic inflammation. PLOS ONE 2016; **11**:e0146744.

47 Wong PK, Quinn JM, Sims NA, van Nieuwenhuijze A, Campbell IK, Wicks IP. Interleukin-6 modulates production of T lymphocyte-derived cytokines in antigen-induced arthritis and drives inflammation-induced osteoclastogenesis. Arthritis Rheum 2006; **54**:158–68.

48 Chao CC, Chen SJ, Adamopoulos IE *et al.* Structural, cellular, and molecular evaluation of bone erosion in experimental models of rheumatoid arthritis: assessment by μCT, histology, and serum biomarkers. Autoimmunity 2010; **43**:642–53.

49 Nishida S, Tsurukami H, Sakai A *et al.* Stage-dependent changes in trabecular bone turnover and osteogenic capacity of marrow cells during development of type II collagen-induced arthritis in mice. Bone 2002; **30**:872–9.

50 Richter J, Capková K, Hříbalová V *et al.* Collagen-induced arthritis: severity and immune response attenuation using multivalent N-acetyl glucosamine. Clin Exp Immunol 2014; **177**: 121–33.

Supporting information

Additional Supporting information may be found in the online version of this article at the publisher's web-site:

Fig. S1. Expression of early osteoclast-specific genes in osteoclastogenic cultures of mice with collagen-induced arthritis. Expression of early osteoclast-specific differentiation genes (*Rank* and *Csf1r*) in bone marrow (BM)-derived and spleen (SPL)-derived osteoclastogenic cultures from control mice (ctrl) and mice with early arthritis (CIA, day 40). *Rank* = receptor activator of nuclear factor κB; *Csf1r* = colony stimulating factor 1 receptor (CD115/cFms). Relative RNA quantities were presented as mean ± standard deviation ($n = 4$–6 wells per group). *Biologically significant difference in the expression ($\geq$ 100%) in comparison to the respective control group.